Photophysical characteristics of 4,4'-bis(N-carbazolyl)tolan derivatives and their application in organic light emitting diodes

Ohkita, Masakazu
Graduate School of Materials Science and Engineering, Nagoya Institute of Technology

Endo, Ayataka
Center for Future Chemistry, and Center for Organic Photonics and Electronics Research (OPERA), Kyushu University

Sumiya, Kimihiro
Graduate School of Materials Science and Engineering, Nagoya Institute of Technology

Nakanotani, Hajime
Center for Future Chemistry, and Center for Organic Photonics and Electronics Research (OPERA), Kyushu University

他

出版情報：Journal of Luminescence. 131 (7), pp.1520-1524, 2011-07. Elsevier
バージョン：

Photophysical characteristics of 4,4'-bis(*N*-carbazolyl)tolan derivatives and their application in organic light emitting diodes

Masakazu Ohkita[a], Ayataka Endo[b], Kimihiro Sumiya[a], Hajime Nakanotani[b], Takanori Suzuki[c], and Chihaya Adachi[b,*]

[a] *Graduate School of Materials Science and Engineering, Nagoya Institute of Technology, Nagoya 466-8555, Japan*

[b] *Center for Future Chemistry, and Center for Organic Photonics and Electronics Research (OPERA), Kyushu University, Fukuoka 819-0395, Japan*

[c] *Division of Chemistry, Graduate School of Science, Hokkaido University, Sapporo 060-0810, Japan*

* Corresponding author. Tel. : +81-92-802-3306; fax : +81-92-802-3306.

E-mail address: adachi@cstf.kyushu-u.ac.jp

Abstract: 4,4'-Bis(*N*-carbazolyl)tolan (**BCT**) and 4,4'-bis[*N*-(3,6-di-*t*-butyl)carbazolyl]tolan (**BCT-*t*-Bu**) were synthesized as π-expanded analogues of 4,4'-bis(*N*-carbazolyl)biphenyl. Their photophysical characteristics both in solution and films were thoroughly investigated. Interestingly,

the phosphorescence spectrum of **BCT** was significantly medium dependent, and the emission maximum was red-shifted by 131 nm from 489 nm in solution at 77K to 620 nm in a deposited film at 5K, suggesting the presence of strong intermolecular interactions in the film. **BCT** and **BCT-*t*-Bu** were found to be useful as host materials for fluorescence-based organic light emitting diodes (OLEDs). However, their low triplet energy levels in films negated their potential to act as hosts in phosphorescence-based OLEDs.

Keywords: Carbazole; Acetylene; Photophysical properties; Organic light emitting diodes; Host materials.

1. Introduction

Carbazole-based π-electron systems have attracted considerable attention in materials science because of their unique light emitting [1,2], carrier transporting [3,4] and photorefractive [5,6] properties, which may find application in organic electronic and optoelectronic devices. 4,4'-Bis(*N*-carbazolyl)biphenyl (**CBP**) has been widely used as a host material for carrier transport and recombination host in organic light-emitting diodes (OLEDs) because of its excellent bipolar carrier transport ability, high thermal stability and comparatively high triplet energy level [7]. In this study, we developed new carbazole-based functional materials by structurally modifying **CBP**. 4,4'-Bis(*N*-carbazolyl)tolan (**BCT**), in which the central biphenyl unit of CBP is replaced by a

diphenylacetylene (tolan) moiety (Scheme 1), was synthesized to clarify the influence of the acetylene spacer. 4,4'-Bis[*N*-(3,6-di-*tert*-butyl)carbazolyl]tolan (**BCT-*t*-Bu**) was also prepared. The synthesis and photophysical characteristics of **BCT** and **BCT-*t*-Bu**, together with their behavior in OLEDs as carrier transport and recombination host materials are reported.

2. Experimental

BCT was synthesized in 67% yield by Pd-catalyzed coupling of carbazole with 4,4'-dibromotolan [8]. A mixture of 4,4'-dibromotolan (336 mg, 1.0 mmol), carbazole (350 mg, 2.1 mmol), potassium carbonate (830 mg, 6.0 mmol), and palladium acetate (22 mg, 0.1 mmol) in toluene (15 mL) was refluxed under nitrogen for 24 h. After the mixture was cooled to room temperature, the toluene was removed under reduced pressure. The residue was diluted with dichloromethane, washed with water, dried over Na_2SO_4, and purified by chromatography on silica gel (chloroform) followed by recrystallization from toluene to afford **BCT** (341 mg, 67%) as colorless crystals: Mp 312 ºC; ^{1}H NMR (300 MHz, $CDCl_3$) δ 7.29-7.35 (m, 4 H), 7.42-7.51 (m, 8 H), 7.62 (AA'BB', 4 H), 7.82 (AA'BB', 4 H), 8.18 (d, J = 7.7 Hz, 4 H); IR (KBr) 3049, 1602, 1518, 1450, 1226 cm^{-1}; MS (MALDI-TOF) *m/z* 508 (M^+). Anal. Calcd for $C_{38}H_{24}N_2$: C, 89.74; H, 4.76; N, 5.51. Found: C, 89.74; H, 4.77; N, 5.35. **BCT-*t*-Bu** was synthesized in a 69% yield in the same manner by Pd-catalyzed coupling of 3,6-di-*t*-butylcarbazole [9] with 4,4'-dibromotolan. Unexpectedly, **BCT-*t*-Bu** was found to be quite insoluble in common organic solvents, and its low

solubility hampered full spectroscopic characterization: MS (MALDI-TOF) *m*/*z* 709 (M^+). Anal. Calcd. for $C_{52}H_{56}N_2$: C, 88.48; H, 7.70; N, 3.82. Found: C, 88.39; H, 7.57; N, 3.69.

Single crystals of **BCT** suitable for analysis by X-ray diffraction were obtained by slow evaporation of a solution of **BCT** in toluene. All measurements were made on a Rigaku/MSC Mercury CCD diffractometer with graphite monochromated Mo-Kα radiation. A total of 5580 unique reflections ($2\theta_{max}$ = 54.96°) were collected, of which 3853 observed reflections were used in the structure solution (direct methods) and refinement (full-matrix least-squares) to give a final *R* of 0.062. Crystal data for **BCT**: $C_{38}H_{24}N_2$, M = 508.59, colorless plate, 0.40 × 0.20 × 0.05 mm, monoclinic, space group $P2_1/c$ (No. 14), D_c = 1.317 g cm^{-3}, a = 5.4070(7), b = 34.756(5), c = 14.084(2) Å, β = 97.2367(9)°, V = 2625.6(6) $Å^3$, Z = 4, T = 123K, μ = 0.76 cm^{-1}.

Cyclic voltammetry was performed in benzonitrile (PhCN) using 0.1 mol/dm^3 tetrabutylammonium perchlorate as the supporting electrolyte. Fluorescence and phosphorescence spectra were recorded of an EPA (diethyl ether/isopentane/ethanol = 5: 5: 2 v/v) solution at a concentration of 10^{-5} mol/dm^3 at 77K and of vacuum deposited films, which were prepared by thermal evaporation under high vacuum (10^{-4} Pa), at 5K. Here note that the vacuum deposited films of **BCT** and **BCT-*t*-Bu** showed uniform films, indicating the formation of amorphous morphologies. PL quantum yields (Φ_{PL}) were determined using an absolute PL quantum yield measurement system (C9920-02, Hamamatsu Photonics). Transient PL characteristics were determined using a streak camera system (C4334, Hamamatsu Photonics) with a nitrogen gas laser (excitation wavelength =

337 nm). To fabricate OLED devices, organic and metal layers were deposited by conventional thermal deposition on a clean glass substrate precoated with a 110 nm-thick indium-tin-oxide (ITO) layer. Current density (*I*)-voltage (*V*)-luminance (*L*) characteristics were measured using a semiconductor parameter analyzer (4155C, Agilent Technologies Inc.) connected to a silicon photodiode (1835-C, Newport Co.).

3. Results and discussion

3.1. Photophysical characteristics

Figure 1 shows the fluorescence and phosphorescence spectra of **BCT** and **BCT-*t*-Bu**, together with those of **CBP** as a reference compound. In EPA solution (○), **BCT** (λ_f = 400 nm) exhibits red-shifted fluorescence compared with that of **CBP** (λ_f = 370 nm), consistent with its increased π-conjugation over **CBP**. **BCT-*t*-Bu** exhibits fluorescence at a similar wavelength to **BCT**, meaning introduction of four *t*-butyl groups onto the **BCT** skeleton has a negligible effect on the fluorescence spectrum in an EPA solution. Compared with **CBP** (λ_{phos} = 485 nm), the phosphorescence spectrum of **BCT** (λ_{phos} = 497 nm) also exhibits a slight red shift in EPA solution, while **BCT-*t*-Bu** (λ_{phos} = 460 nm) showed broad structureless emission at a shorter wavelength. In the deposited films (●), the fluorescence maxima of **CBP** (λ_f = 404 nm), **BCT** (λ_f = 440 nm) and **BCT-*t*-Bu** (λ_f = 416 nm) are red-shifted by 34 nm, 40 nm and 17 nm, respectively, compared with those in EPA solution (Table 1), because of the increased intermolecular interactions in the

deposited films. The phosphorescence spectra of the deposited films are also red-shifted compared with those in solution; **CBP** (27 nm), **BCT** (131 nm) and **BCT-*t*-Bu** (52 nm).

The molecular interactions in the compounds can be also understood by comparing the fluorescence quantum yield (Φ_f) in solution and solid films. Table 1 summarizes the Φ_f values of **CBP**, **BCT** and **BCT-*t*-Bu** in solution and deposited films. Although Φ_f is very high for **BCT** and **BCT-*t*-Bu** in solution, a pronounced decrease in Φ_f was observed for both the solid films of **BCT** (Φ_f=0.68) and **BCT-*t*-Bu (**Φ_f=0.38). Although we expected a smaller decrease of Φ_f in the solid film of **BCT-*t*-Bu** compared with that of **BCT** due to the presence of bulky t-butyl groups which hinder concentration quenching, quite opposite result was obtained, indicating the presence of unknown molecular interactions in these molecules.

Single crystal X-ray diffraction analysis of **BCT** revealed that the tolan moiety is almost planar in the solid state. The dihedral angle between the two benzene rings is 3.8° while the carbazole units in **BCT** are twisted about the central tolan skeleton by 56.0° and 59.5° in the same direction (Fig. 2a). The crystal packing of **BCT** shows the characteristic herringbone structure caused by C-H···π interactions (Fig. 2b), and no significant π-stacking is observed in the crystal packing. Unfortunately, we have been unable to obtain single crystals of **BCT-*t*-Bu** suitable for study by X-ray diffraction.

Based on these results, the marked red shift of 131 nm observed for **BCT** can be attributed to specific intermolecular interactions of **BCT** in the solid film, presumably caused by its increased

molecular planarity over that of CBP. Further, the inter-molecular interaction of C-H···π interaction in a **BCT** film would induce a large polarization of the triplet excited state, while the steric hindrance of the bulky *t*-butyl groups in **BCT-*t*-Bu** may prevent such intermolecular interactions, resulting in a smaller red shift.

Next, the compounds were used as hosts in host-guest films containing fluorescent and phosphorescent dopants. Highly fluorescent 1,4-dinitrile-2,5-bis(4-(bis(4-methoxyphenyl)amino) styryl)benzene (**BSB-CN**) was doped into **BCT** and **BCT-*t*-Bu** host layers to confirm their potential to act as host layers in OLEDs. As summarized in Table 2, at a doping concentration of 6 wt% **BSB-CN**, slightly higher values of Φ_{PL} are obtained for **BCT** and **BCT-*t*-Bu** host layers compared with that obtained using **CBP**, suggesting that the tolan derivatives would be useful host materials for fluorescence-based OLEDs. Figure 3 shows the absorption and fluorescence spectra of **BSB-CN** in a toluene solution (10^{-5} mol/l). The spectral overlap between the absorption spectrum of **BSB-CN** and the fluorescence spectra of **CBP**, **BCT** and **BCT-*t*-Bu** films as shown in Fig. 1 is significant, ensuring the perfect energy transfer from the host layers into **BSB-CN**. We note that the fluorescence spectra of the all co-deposited films showed only **BSB-CN** emission. Thus, the small difference of Φ_{PL} in the doped films would be due to the other factors such as dispersion condition of **BSB-CN** molecules in the host layers.

The tolan derivatives were also tested as host materials in phosphorescence-based OLEDs containing 6wt% tris(2-phenylpyridinato)iridium (III) ($Ir(ppy)_3$) as a phosphorescent emitter.

Although Φ_{PL} = 90 ± 3% for $Ir(ppy)_3$ was obtained using a **CBP** host, a reduced value of Φ_{PL} = 66 ± 3% was achieved with a **BCT-*t*-Bu** host layer and complete quenching of $Ir(ppy)_3$ emission (Φ_{PL} < 1%) was found with a **BCT** host layer. These results are consistent with the triplet energies estimated from the phosphorescence spectra of the compounds. In case of **BCT-*t*-Bu**, the double exponential decay curve of the $Ir(ppy)_3$: **BCT-*t*-Bu** film with τ_1 = 0.55 μs and τ_2 = 1.75 μs also suggests imperfect energy confinement of the triplet excitons of $Ir(ppy)_3$ because of the comparable triplet energies of the host layer and the guest molecule. Here, we note that although Φ_{PL} is 66 ± 3% at room temperature, it increased significantly to 90 ± 3% at 5K. Thus, the energy levels of **BCT-*t*-Bu** and $Ir(ppy)_3$ compete with each other. At low temperatures, the triplet excitons of $Ir(ppy)_3$ cannot overcome the potential barrier between $Ir(ppy)_3$ and **BCT-*t*-Bu**, leading to a very high Φ_{PL}. In addition, the red phosphor 2-(2-benzo[4,5-a]thienyl)pyridinato-N,C^3)iridium (acetylacetone) ($Btp_2Ir(acac)$) was doped into the different host materials. Compared with Φ_{PL} = 40 ± 3% with a **CBP** host, slightly lower Φ_{PL} values of 29 ± 3% and 24 ± 3% were obtained using **BCT** and **BCT-*t*-Bu** as host layers indicating imperfect confinement of the triplet excitons of $Btp_2Ir(acac)$ or the presence of unwanted interactions between the host and guest molecules.

3.2. OLED characteristics using the tolan derivatives as host materials

The half-wave oxidation ($E_{1/2}^{ox}$) potentials of **BCT** and **BCT-*t*-Bu** in PhCN were determined to be 1.30 V and 1.22 V (*vs.* SCE), respectively. From the observed oxidation potential

coupled with the absorption onset, the highest occupied molecular orbital (HOMO) and the lowest unoccupied molecular orbital (LUMO) levels of **BCT** were estimated to be 5.7 eV and 2.4 eV, respectively. In a same manner, the HOMO and LUMO levels of **BCT-*t*-Bu** were estimated to be 5.6 eV and 2.4 eV, respectively. Because these values are comparable to those of **CBP**, the tolan derivatives **BCT** and **BCT-*t*-Bu** show potential to act as host materials in OLEDs.

To evaluate the ability of **BCT** and **BCT-*t*-Bu** to act as host materials in fluorescent OLEDs, we prepared devices with the structure ITO (110 nm) / α-NPD (30 nm) / 6wt% BSB-CN: host (20 nm) / BCP (20 nm) / Alq_3 (30 nm) / MgAg (100 nm) / Ag (10 nm). α-NPD, Alq_3 and BCP are *N,N'*-diphenyl-*N,N'*-bis(1-naphthyl)-1,10-biphenyl-4,4'-diamine as a hole transport layer, tris(8-hydroxyquinolinato)aluminum(III) as an emitter layer and 2,9-dimethyl-4,7-diphenyl-1,10-phenanthroline as an electron transport layer, respectively. As shown in Fig. 3, the device containing CBP as a host showed a maximum external EL quantum efficiency (η_{ext}) of 2.3% while the devices containing **BCT** and **BCT-*t*-Bu** host layers showed slightly higher η_{ext} values of 3.0% and 2.6%, respectively. Here, we note that a slightly lower drive voltage was required in the devices containing the tolan derivatives as the host material compared with that needed in the **CBP** device (Inset of Fig. 3). As suggested from the results of the photoluminescence study, probably the tighter molecular packing of **BCT** compared with that of **CBP** would lead to better carrier transport ability in the solid films.

Phosphorescence-based devices with the configuration ITO (110 nm) / TPD (50 nm) /

phosphor: host (20 nm) / BCP (10 nm) / Alq_3 (30 nm) / MgAg (100 nm) / Ag (10 nm) were also examined. Here, TPD is *N,N'*-bi(3-methylphenyl)-*N,N'*-bis(phenyl)benzidine, which acts as a hole transport layer. With a **BCT** host layer η_{ext}=4.5%, while using a **BCT-*t*-Bu** host layer gave η_{ext}=2.0% when the dopant phosphor was $Btp_2Ir(acac)$. In contrast, the **CBP** host layer gave a higher η_{ext} of 7.0% for the same dopant. Furthermore, when the green phosphor $Ir(ppy)_3$ was used as the dopant, η_{ext} decreased significantly to 0.l % using a **BCT** host layer and 3.8% using a **BCT-*t*-Bu** host layer(Fig. 4). This indicates that the tolan derivatives are not promising for use as host layers in phosphorescent devices.

4. Conclusion

The photoluminescence characteristics of CBP derivatives **BCT** and **BCT-*t*-Bu** were studied both in solution and in films. It was found that these materials are useful for host materials in fluorescence-based OLEDs, performing better than the traditional host material CBP. However, the low triplet energy levels of **BCT** and **BCT-*t*-Bu** in their films means they behave poorly as host materials in phosphorescence-based OLEDs.

Acknowledgments

This work was partially supported by a Grant-in-Aid for Scientific Research (C) (No.21550041) and a Grant-in-Aid for the Global COE Program, "Science for Future Molecular Systems" from the Ministry of Education, Culture, Sports, Science, and Technology, Japan. We

thank Professor Tamotsu Inabe (Hokkaido University) for use of an X-ray structure diffractometer. We are grateful to the Research Foundation for the Electrotechnology of Chubu and the Tatematsu Foundation for financial support.

References

[1] M. Sigalov, A. Ben-Asuly, L. Shapiro, A. Ellern, V. Khodorkovsky, Tetrahedron Lett. 41 (2000), 8573.

[2] Y. Liu, M. Nishiura, Y. Wang, Z. Hou, J. Am. Chem. Soc. 128 (2006), 5592.

[3] J. Kido, K. Hongawa, K. Okuyama, K. Nagai, Appl. Phys. Lett. 63 (1993), 2627.

[4] H.-H. Chou and C.-H. Cheng, Adv. Mater. 22 (2010) 2468.

[5] Y. Zhang, L. Wang, T. Wada, H. Sasabe, Appl. Phys. Lett. 70 (1997), 2949.

[6] Y. Zhang, T. Wada, H. Sasabe, J. Mater. Chem. 8 (1998), 809.

[7] M. A. Baldo, S. Lamansky, P. E. Burrows, M. E. Thompson, S. R. Forrest, Appl. Phys. Lett. 75 (1999), 4.

[8] S. M. Waybright, K. McAlpine, M. Laskoski, M. D. Smith, U. H. F. Bunz, J. Am. Chem. Soc. 124 (2002), 8661.

[9] T. Xu, R. Lu, X. Liu, X. Zheng, X. Qiu, Y. Zhao, Org. Lett. 9 (2007), 797.

Figure captions

Scheme 1: Molecular structures of **CBP**, **BCT**, **BCT-t-Bu**, BSB-CN, $Ir(ppy)_3$, and $Btp_2Ir(acac)$.

Fig. 1: Fluorescence and phosphorescence spectra of **CBP**, **BCT** and **BCT-*t*-Bu** in an EPA solution (10^{-5} mol/l) (○) and deposited films (●).

Fig. 2: X-ray molecular structure (a) and crystal packing (b) of **BCT**.

Fig. 3: Fluorescence and phosphorescence spectra of **BSB-CN** in a toluene solution (10^{-5} mol/l).

Fig. 4: *J*-η_{ext} characteristics of devices with the structure ITO (110 nm) /α-NPD (30 nm) / 6wt% **BSB-CN**: host (20 nm) / BCP (20 nm) / Alq_3 (30 nm) / MgAg (100 nm) / Ag (1 0 nm) with a host layer of **CBP** (○), **BCT** (□) and **BCT-*t*-Bu** (▲). The inset shows the corresponding *J*-*V* characteristics of the OLEDs.

Fig. 5: J-η_{ext} characteristics of devices with the structure ITO (110 nm) / TPD (50 nm) / EML (20 nm) / BCP (10 nm) / Alq_3 (30 nm) / MgAg (100 nm) / Ag (10 nm) devices with an EML of 6w% $Ir(ppy)_3$:1 (■), 6wt% $Ir(ppy)_3$:2 (▲), 6wt% $Btp_2Ir(acac)$:**BCT** (□) and 6wt% $Btp_2Ir(acac)$:**BCT-*t*-Bu**

(Δ).

Table 1: λ_{peak}, PL quantum efficiency of CBP, BCT and BCT-t-Bu in solution and vacuum deposited films

	(in solution)		(in solid films)	
Material	λ (nm)	Φ_{PL} (%)	λ (nm)	Φ_{PL} (%)
CBP	370	80± 3	404	60± 3
BCT	400	86± 3	440	70± 3
BCT-*t*-Bu	399	97± 3	416	40± 3

Table 2: λ_{peak}, PL quantum efficiency and transient life time of co-deposited films

Guest material	Host material	λ (nm)	Φ_{PL} (%)	τ (ns)
BSB-CN	CBP	559	65 ± 3	1.5 ± 0.3
	BCT		71 ± 3	1.5 ± 0.3
	BCT-t-Bu		77 ± 3	1.5 ± 0.3

Guest material	Host material	λ (nm)	Φ_{PL} (%)	τ (μs)
$Ir(ppy)_3$	CBP	511	90 ± 3	1.0 ± 0.3
	BCT		< 1	-
	BCT-t-Bu		66 ± 3	0.6, 1.8 ± 0.3
$Btp_2Ir(acac)$	CBP	617	40 ± 3	5.4 ± 0.3
	BCT		29 ± 3	3.0, 11.0 ± 0.3
	BCT-t-Bu		24 ± 3	5.5 ± 0.3

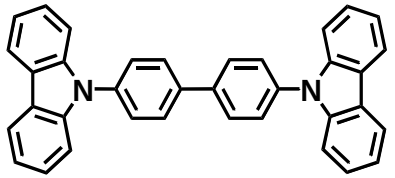

CBP

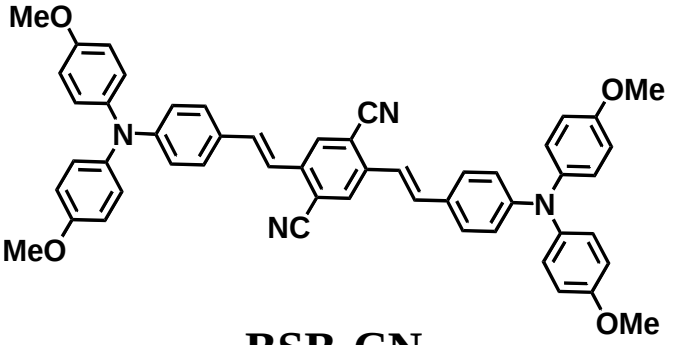

BSB-CN

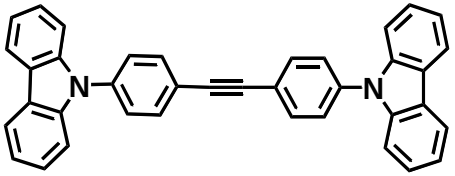

BCT

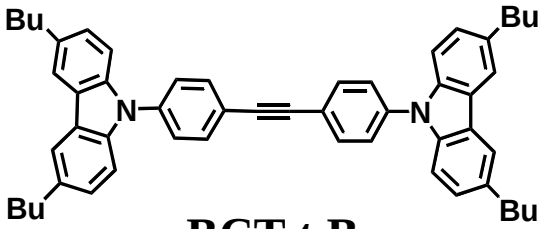

BCT-*t*-Bu

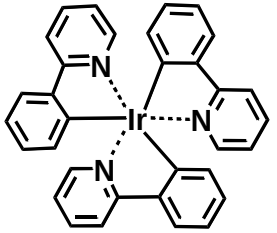

Ir(ppy)$_3$

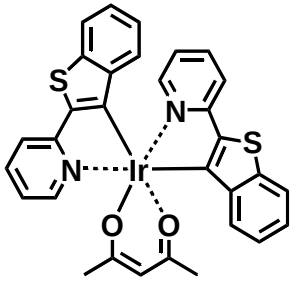

Btp$_2$Ir(acac)

Scheme 1

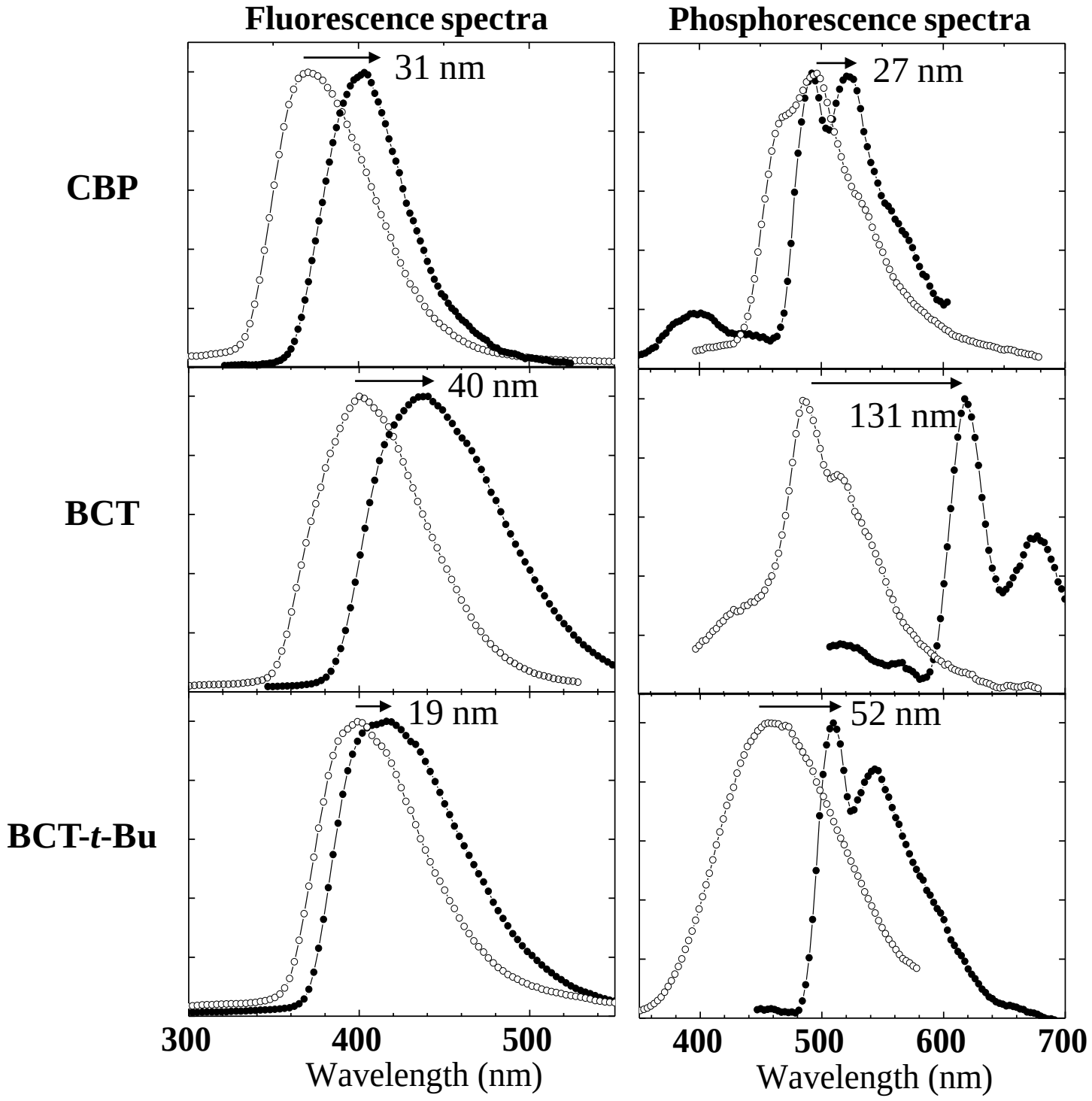
Fluorescence spectra
Phosphorescence spectra
CBP
BCT
BCT-t-Bu
31 nm
27 nm
40 nm
131 nm
19 nm
52 nm
300
400
500
400
500
600
700
Wavelength (nm)
Wavelength (nm)

Figure 1

(a)

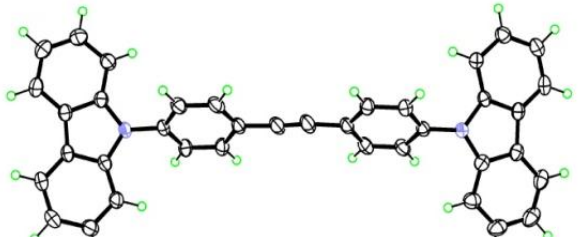

(b)

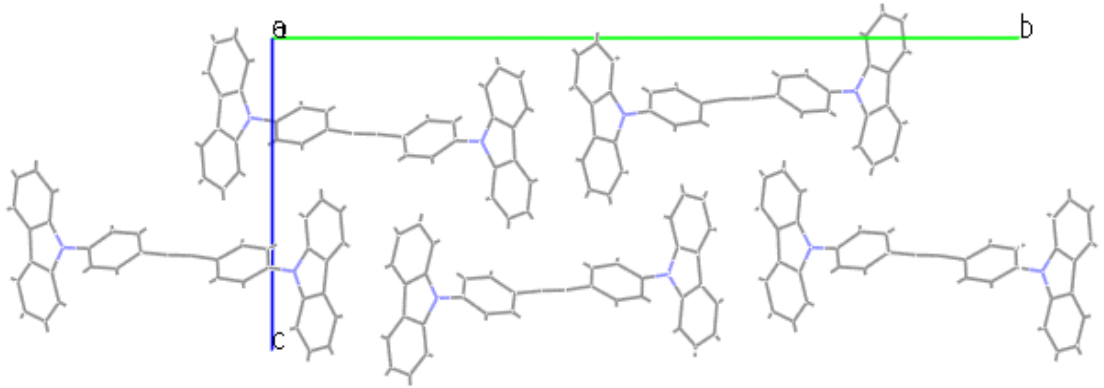

Figure 2

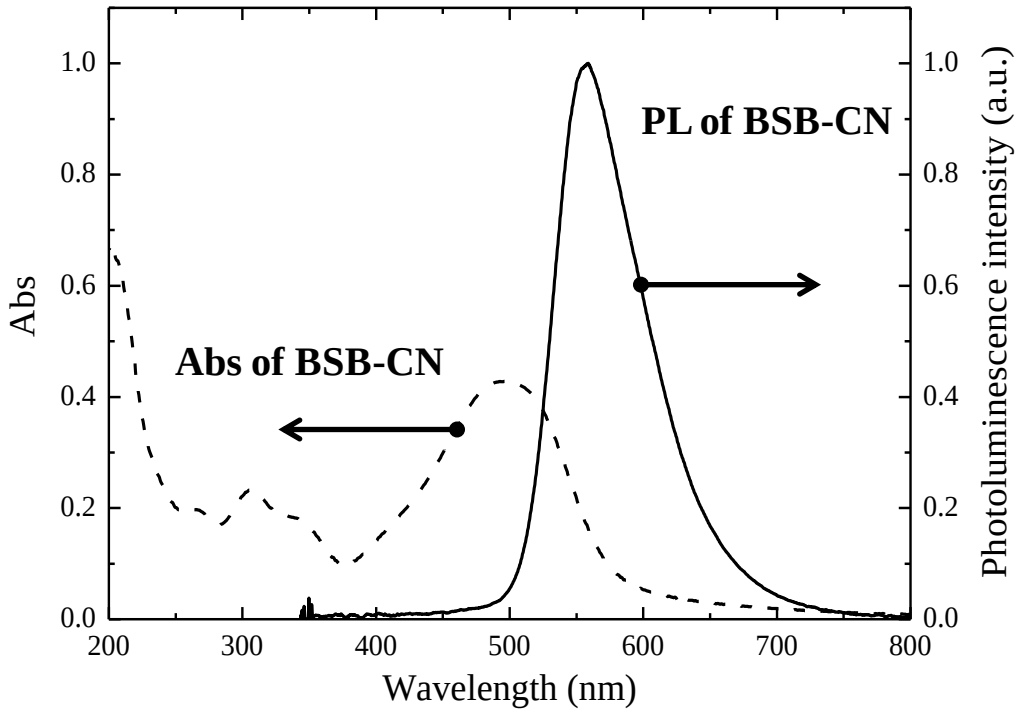
PL of BSB-CN
Abs of BSB-CN
Abs
Photoluminescence intensity (a.u.)
Wavelength (nm)
0.0
0.2
0.4
0.6
0.8
1.0
200
300
400
500
600
700
800

Figure 3

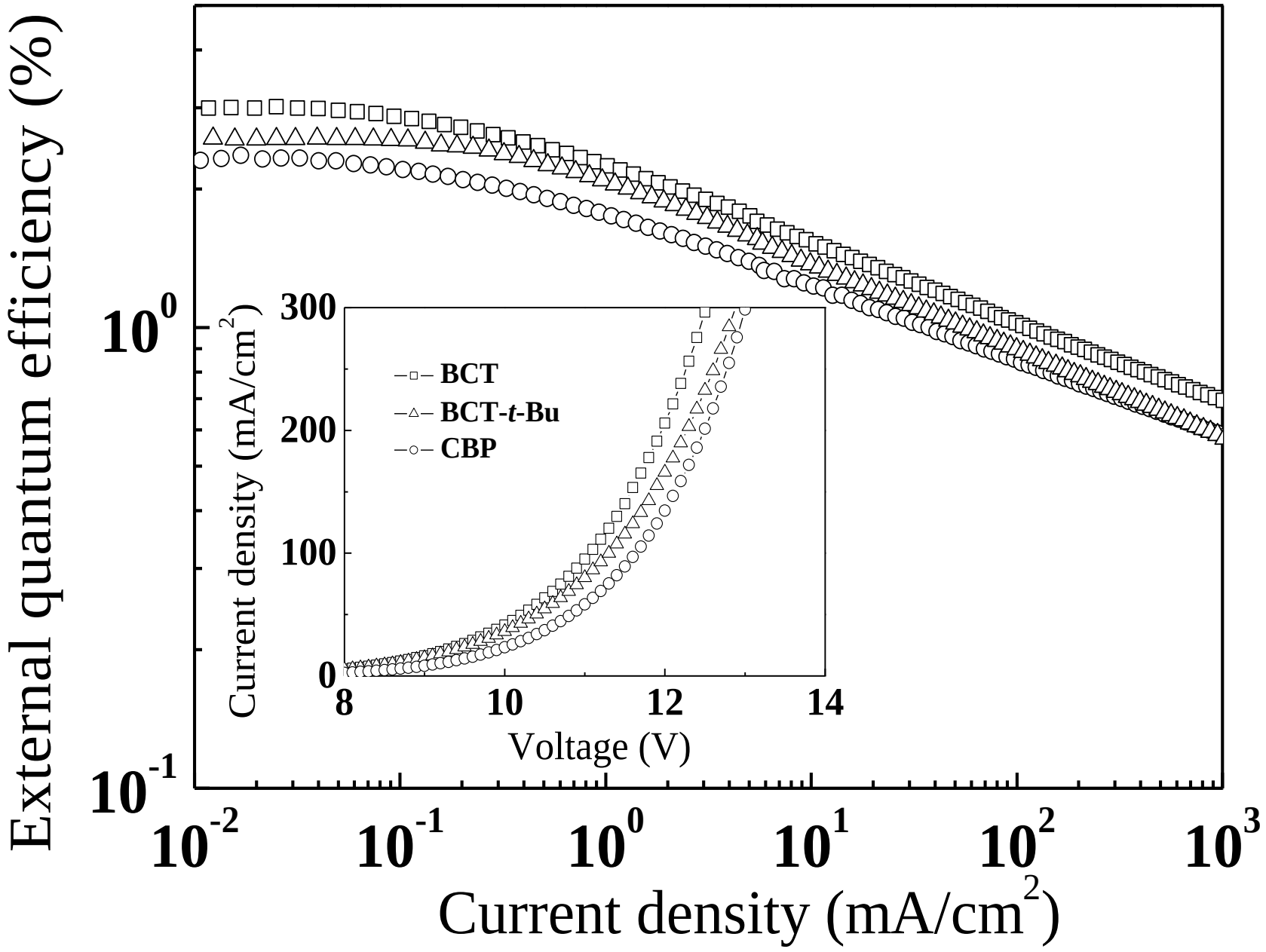
External quantum efficiency (%)
10^0
10^-1
10^-2
10^-1
10^0
10^1
10^2
10^3
Current density (mA/cm^2)
300
200
100
0
8
10
12
14
Voltage (V)
Current density (mA/cm^2)
BCT
BCT-t-Bu
CBP

Figure 4

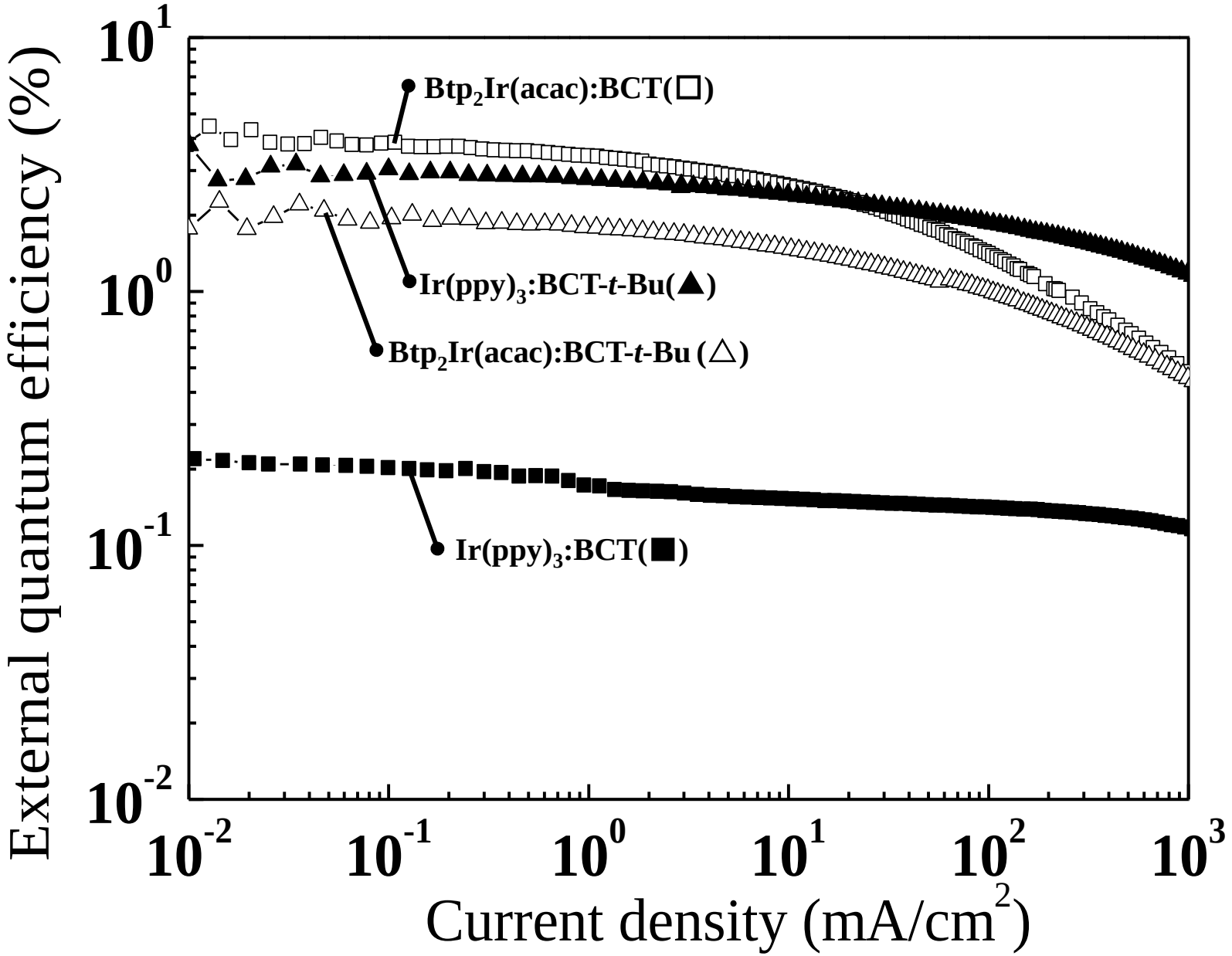
External quantum efficiency (%)
10^1
10^0
10^-1
10^-2
Btp2Ir(acac):BCT(□)
Ir(ppy)3:BCT-t-Bu(▲)
Btp2Ir(acac):BCT-t-Bu (△)
Ir(ppy)3:BCT(■)
10^-2
10^-1
10^0
10^1
10^2
10^3
Current density (mA/cm^2)

Figure 5